JACS
JOURNAL OF THE AMERICAN CHEMICAL SOCIETY

ARTICLE

pubs.acs.org/JACS

Promiscuity of Carbonic Anhydrase II. Unexpected Ester Hydrolysis of Carbohydrate-Based Sulfamate Inhibitors

Marie Lopez,[†] Hoan Vu,[†] Conan K. Wang,[†] Maarten G. Wolf,[‡] Gerrit Groenhof,[‡] Alessio Innocenti,[§] Claudiu T. Supuran,[§] and Sally-Ann Poulsen*[,†]

[†]Eskitis Institute for Cell and Molecular Therapies, Griffith University, Nathan, Queensland 4111, Australia

[‡]Biomolecular Chemistry Group, Theoretical and Computational Biophysics Department, Max Planck Institute of Biophysical Chemistry, Am Fassberg 11, 37077 Göttingen, Germany

[§]Polo Scientifico, Laboratorio di Chimica Bioinorganica, Università degli Studi di Firenze, Via della Lastruccia 3, 50019 Sesto Fiorentino, Florence, Italy

Supporting Information

ABSTRACT: Carbonic anhydrases (CAs) are enzymes whose endogenous reaction is the reversible hydration of CO_2 to give HCO_3^- and a proton. CA are also known to exhibit weak and promiscuous esterase activity toward activated esters. Here, we report a series of findings obtained with a set of CA inhibitors that showed quite unexpectedly that the compounds were both inhibitors of CO_2 hydration and substrates for the esterase activity of CA. The compounds comprised a monosaccharide core with the C-6 primary hydroxyl group derivatized as a sulfamate (for CA recognition). The remaining four sugar hydroxyl groups were acylated. Using protein X-ray crystallography, the crystal structures of human CA II in complex with four of the sulfamate inhibitors were obtained. As expected, the four structures displayed the canonical CA protein−sulfamate interactions. Unexpectedly, a free hydroxyl group was observed at the anomeric center (C-1) rather than the parent C-1 acyl group. In addition, this hydroxyl group is observed axial to the carbohydrate ring while in the parent structure it is equatorial. A mechanism is proposed that accounts for this inversion of stereochemistry. For three of the inhibitors, the acyl groups at C-2 or at C-2 and C-3 were also absent with hydroxyl groups observed in their place and retention of stereochemistry. With the use of electrospray ionization−Fourier transform ion cyclotron resonance−mass spectrometry (ESI−FTICR−MS), we observed directly the sequential loss of all four acyl groups from one of the carbohydrate-based sulfamates. For this compound, the inhibitor and substrate binding mode were further analyzed using free energy calculations. These calculations suggested that the parent compound binds almost exclusively as a substrate. To conclude, we have demonstrated that acylated carbohydrate-based sulfamates are simultaneously inhibitor and substrate of human CA II. Our results suggest that, initially, the substrate binding mode dominates, but following hydrolysis, the ligand can also bind as a pure inhibitor thereby competing with the substrate binding mode.

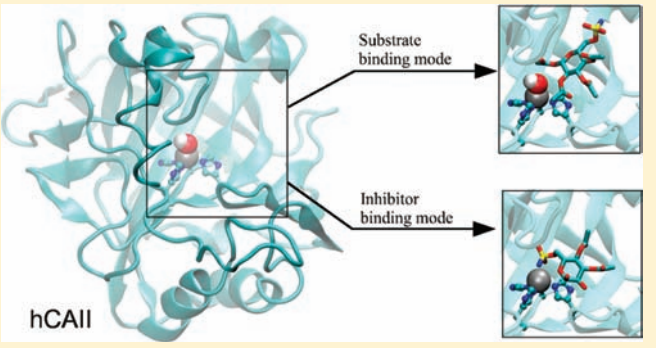

INTRODUCTION

Carbonic anhydrases (CAs, EC 4.2.1.1) are zinc metalloenzymes that catalyze the reversible hydration of carbon dioxide (CO_2) to generate bicarbonate anion (HCO_3^-) and a proton (H^+).[1] This equilibrium contributes to a range of physiological functions that involve the production, transport, and consumption of CO_2, H^+, and HCO_3^-.[1a] Two CA isozymes (IX and XII) have validated potential for targeting the development of personalized, first-in-class cancer chemotherapies and selective CA inhibitors are needed.[1] The catalytic domain of CAs comprises a tetrahedral Zn^{2+} cation coordinated to the side chain imidazole of three histidine residues. The fourth Zn^{2+} ligand is the substrate H_2O molecule. Coordination to Zn^{2+} lowers the pK_a of the substrate H_2O molecule to ∼6.8 (the pK_a of bulk water is ∼14) and this facilitates formation of zinc bound hydroxide at physiological pH.[1b] Hydroxide is the nucleophile that reacts with CO_2; the net effect of CA activity is hydration of CO_2, Scheme 1a.[1b]

There are growing numbers of promiscuous activities reported for enzymes, with both substrate promiscuity (catalysis of the same chemical reaction for a range of different substrates) and catalytic promiscuity (catalysis of chemically distinct reactions, involving different transition states) reported.[2] hCA II (h = human) exhibits weak and promiscuous esterase activity toward activated esters such as *p*-nitrophenyl acetate ($k_{cat}/K_M \sim 10^3\ M^{-1}\ s^{-1}$ versus $\sim 10^8\ M^{-1}\ s^{-1}$ for CO_2 hydration).[3] The physiological relevance of CAs catalytic esterase activity is unknown; it is however halted in the presence of CA inhibitors, indicating that the zinc-hydroxide

Received: August 25, 2011
Published: September 29, 2011

 © 2011 American Chemical Society

Scheme 1. Representation of the Catalytic Cycle for Human CA II Catalyzed (a) Hydration of CO_2 to HCO_3^- and H^+;[1b] and (b) Ester Hydrolysis to Carboxylic Acid and Alkoxide[a]

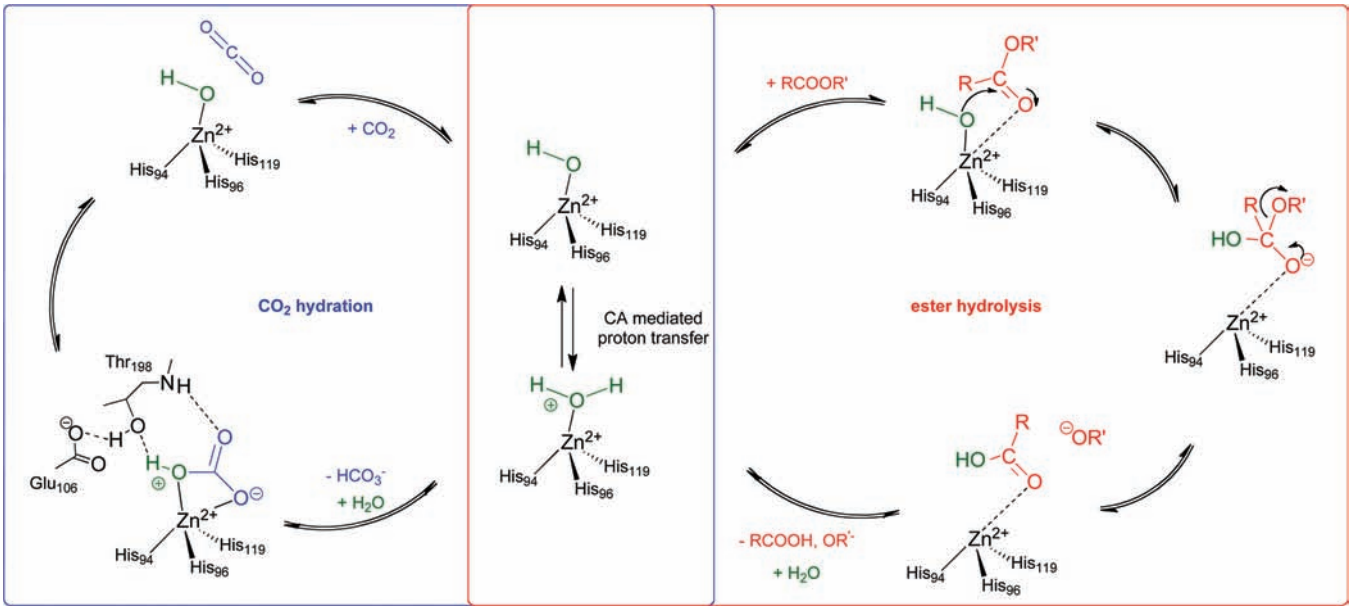

[a] The zinc bound hydroxide is the active form of the enzyme.

Scheme 2. Other CA Catalyzed Hydration Reactions

(a) $O{=}C{=}NH + H_2O \leftrightarrows H_2NCOOH$

(b) $NH{=}C{=}NH + H_2O \leftrightarrows H_2NCONH_2$

(c) $RCHO + H_2O \leftrightarrows RCH(OH)_2$

mechanism responsible for the CO_2 hydration activity by CAs is also responsible for the esterase activity, Scheme 1b.[4] CAs have also been reported to catalyze a number of other hydration reactions, again for which the physiological relevance is unknown.[5] The hydration substrates are typically simple in structure and reactions include (i) the hydration of cyanate to carbamic acid (Scheme 2a); (ii) the hydration of cyanamide to urea (Scheme 2b); and (iii) the hydration of aldehydes to gem-diols (Scheme 2c).[6]

The implied target for CA inhibitors is the active site Zn^{2+} cation and zinc binding groups (ZBGs), especially sulfonamides and sulfamates, feature prominently in small molecule drug design against CAs.[1a] The anion form of these ZBGs, $R\text{-}SO_2NH^-$ and $R\text{-}OSO_2NH^-$, respectively, where R is typically an aromatic moiety, anchors them to the active site Zn^{2+}, in place of endogenous water/hydroxide. For $R\text{-}SO_2NH^-$, the sulfonamide NH forms a hydrogen bond with the side chain oxygen of Thr_{198}, while one oxygen atom accepts a hydrogen bond from the backbone NH of Thr_{198}, Figure 1b.[1b] These canonical interactions are shared by sulfamates, and together, these inhibitor−CA II interactions are evidenced in approximately 120 X-ray structures of ligands in complex with hCA II in the Protein Data Bank.

Binding of $R\text{-}SO_2NH^-$ and $R\text{-}OSO_2NH^-$ mimics the transition state structure of CA bound to bicarbonate, where the bicarbonate OH oxygen atom coordinates to the active site Zn^{2+}; the bicarbonate OH group also donates a hydrogen bond to the side chain oxygen of Thr_{198}, while the carbonyl oxygen of bicarbonate

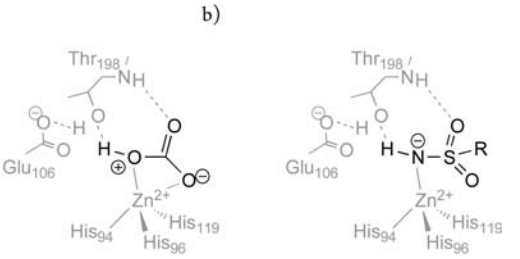

Figure 1. Schematic of the CA active site of catalytically active hCA isozymes showing: (a) the transition state with the active site Zn^{2+} bound to HCO_3^-; and (b) a primary sulfonamide CA inhibitor bound to the active site Zn^{2+}.

accepts a hydrogen bond from the backbone NH of Thr_{198}, Figure 1a.[1b] Small molecule CA inhibitors that do not interact with the zinc ion have been identified only recently, for example, compounds comprising a coumarin scaffold.[7]

In the current study, we present a series of structural observations that were obtained following the analysis of several CA inhibitors in the presence of hCA II using protein X-ray crystallography and bioaffinity mass spectrometry. These CA inhibitors belonged to a novel compound class of carbohydrate-based sulfamates whose carbohydrate hydroxyl groups were either free (−OH) or acylated (−OAcyl). Both biophysical methods provided data that indicated that the sulfamate compounds, in addition to being CA inhibitors, were also substrates for the esterase activity of CA, with the ester groups of the sugar hydrolyzed by CA II. For one of these compounds, both the inhibitor and substrate binding mode were further analyzed using free energy calculations. These calculations suggest that the parent compound binds almost exclusively as a substrate. The various hydrolysis products can also bind as a pure inhibitor, competing with the substrate binding mode.

RESULTS AND DISCUSSION

The esterase activity reported for hCA II with phenyl acetates shows that activity is sensitive to the chemical nature of both the acyl and the phenolic fragments that comprise the ester substrate.[6b] Tawfik demonstrated a linear relationship between the pK_a of the phenolic leaving group and hCA II esterase substrate reactivity with a series of substituted phenyl acetates,[8] Table 1. Their study showed that the ester substrate reactivity falls as the pK_a of the ROH leaving group increases, thus activated esters wherein the pK_a of the product alcohol is low, are the best substrates for the esterase activity of hCA II. 4-Nitrophenyl acetate (pK_a of 4-nitrophenol =7.14) is the most active known hCA II substrate for ester hydrolysis, while 4-methoxyphenyl acetate (pK_a of 4-methoxyphenol =10.29) is ~400-fold less active, Table 1.

The compounds in this study are sulfamates derived from the monosaccharides D-glucose (**1a**−**d**), D-galactose (**2a**−**b**) and D-mannose (**3a**−**b**), Chart 1. The sulfamate moiety is on the C-6 primary hydroxyl group of the monosaccharide, with the remaining four hydroxyl groups either unmodified (**1a**−**3a**) or acylated as acetyl (**1b**−**3b**), propionyl (**1c**), or butyryl (**1d**) ester protecting groups. In a recent contribution, we presented the design, synthesis, and CA inhibition profile of these compounds.[9] These compounds displayed good selectivity for cancer-associated CA isozymes.[9] The hCA II inhibition constants (K_i values) ranged from 11 to 307 nM as determined using a stopped flow assay that monitors the production of H^+ from the CA catalyzed hydration of CO_2, Table 2.[9,10]

Table 1. Relationship of CA II Catalyzed Ester Hydrolysis of Phenyl Acetates with Leaving Groups of Varying pK_a Values[8]

substrate	pK_a	k_{cat}/K_M (M^{-1} s^{-1})
4-nitrophenyl acetate	7.14	2050 ± 162
2,3-difluorophenyl acetate	7.81	1140 ± 62
2,4-difluorophenyl acetate	8.43	133 ± 8
4-chlorophenyl acetate	9.38	53 ± 3
phenyl acetate	10	40 ± 4
4-methoxyphenyl acetate	10.29	5.3 ± 1

Our primary motivation in studying CA inhibitors is therapeutic drug discovery. Given the variable hCA II inhibition profile across this small group of monosaccharide derivatives, differing only by the hydroxyl group acylation profile and the axial/equatorial stereochemistry, we hoped to discern the interactions of these compounds with active site residues of hCA II so as to identify the structural features of these ligands that may be important to directing future medicinal chemistry campaigns against this enzyme class. Protein X-ray structures of native CA with inhibitors can demonstrate with intricate detail how novel small molecule enzyme inhibitors bind in the active site. This structure rich information allows the interpretation of structure−activity relationships (SAR) for drug discovery research campaigns.

To obtain these insights, we thus applied protein X-ray crystallography. Using co-crystallization, crystal structures of hCA II obtained in the presence of the sulfonamide inhibitors **1b**, **1c**, **2b**, and **3b** were obtained at a resolution of 2.0, 1.8, 2.0, and 2.4 Å, respectively. As expected, the four enzyme bound structures displayed the canonical CA protein−sulfamate interactions (similar to Figure 1b). Unexpectedly, however, hydrolysis of inhibitors **1b**, **1c**, **2b**, and **3b** was apparent and hydrolyzed compounds **4**, **5**, **6**, and **7**, respectively, were observed in the crystal structures. For all inhibitors, a free hydroxyl group was observed at the anomeric center (C-1), while hydrolysis of the

Table 2. Enzyme Inhibition Data of hCA II[a] with Carbohydrate-Based Sulfamates 1a−d, 2a,b, 3a,b

compound	K_i (nM)[b]
1a	82
2a	93
3a	104
1b	307
2b	106
3b	11.3
1c	105
1d	114

[a] h = human. [b] Errors in the range of ±5% of the reported value, from three determinations.

Chart 1. Carbonic Anhydrase Inhibitors—Sulfamates Derived from Monosaccharides

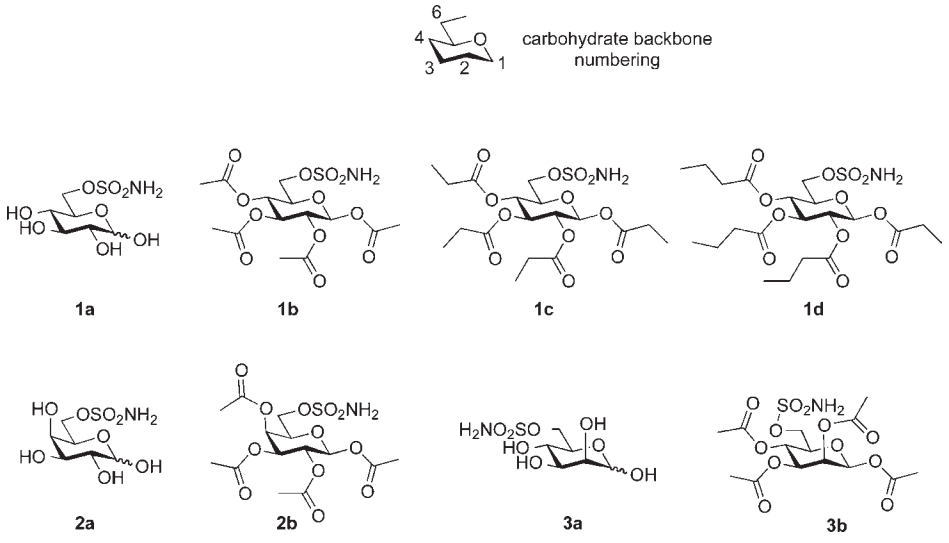

dx.doi.org/10.1021/ja207855c |J. Am. Chem. Soc. 2011, 133, 18452–18462

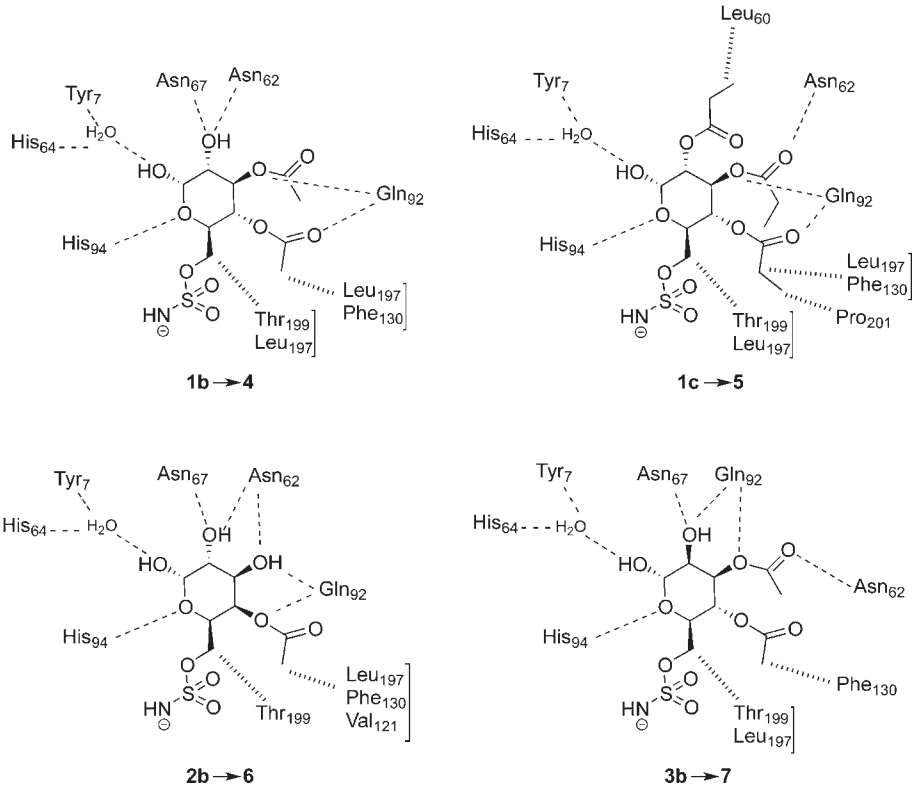

Figure 2. Schematic view of observed ligand interactions from inhibitor-bound hCA II: sulfamate **1b** (compound **4**), **1c** (compound **5**), **2b** (compound **6**), and **3b** (compound **7**) protein crystal structures. The canonical sulfamate interactions (Figure 1b) are not shown for the purpose of clarity. Hydrogen bond interactions are shown as dotted lines, van der Waals interactions as dashed lines. For compound **1c**, the C-1 hydroxyl is observed 95% axial (shown) and 5% equatorial, and the water H-bond is conserved in both anomers.

C-2 acetyl group of **1b** and **3b** and the C-2 and C-3 acetyl groups of **2b** was also apparent (hydroxyl groups were observed at C-1 and C-2 for compounds **4** and **7**, and at C-1, C-2 and C-3 for compound **6**). The C-1 acyl group of the parent inhibitor is equatorial; however, the C-1 hydroxyl group was observed axial to the carbohydrate ring for **4**, **6**, and **7**, while for the propionyl derivative **5**, it was observed 95% axial and 5% equatorial. To investigate the chemical stability of **1b**, **2b**, **3b**, and **1c** in the buffer conditions used for co-crystallization, a solution of each acylated sulfamate compound was prepared in the co-crystallization buffer. No ester hydrolysis was observed for up to 1 month of exposure to buffer and the parent structures remained invariant. These results confirmed the chemical stability of the sugar sulfamates to the buffer conditions used for co-crystallization, showing that no spontaneous hydrolysis of **1b**, **2b**, **3b**, and **1c** in buffer occurs. These results are consistent with the premise that the CA enzyme mediates ester hydrolysis of these inhibitor compounds.

In addition to the canonical sulfamate interactions, the crystal structures of the four sulfamate ligands reveal that there are several additional interactions between the bound ligands and amino acid residues of hCA II, some of which are highly conserved and involve residues that are involved in zinc binding (His_{94}) or proton transfer (His_{64}). The observed hydrolyzed ligands of **1b**, **1c**, **2b**, and **3b** are denoted as compounds **4**, **5**, **6**, and **7**, respectively. For each ligand, the anomeric hydroxyl group interacts indirectly with the side chain hydroxyl of Tyr_7 and the backbone carbonyl of His_{64} through formation of a strong hydrogen bond with an ordered water molecule (i.e., bond distance between 2.47 and 2.65 Å), while the sugar ring oxygen of **4**−**7** interacts with His_{94} through a direct but weaker hydrogen bond (i.e., bond distance between 3.07 and 3.57 Å), Figure 2. There is conservation of a hydrophobic interaction of the methylene group with the Thr_{199} and Leu_{197} (absent only in compound **6**). The C-2 hydroxyl group of **4**, **6**, and **7** forms hydrogen bonds with Asn_{67} and Asn_{62}, while the side chain of Leu_{60} provides hydrophobic contacts with the aliphatic group of the C-2 propionyl substituent of **5**. The C-3 hydroxyl group of **6** forms a hydrogen bond with Asn_{62} and Gln_{92}, while the C-3 alkyl group oxygen of **4**, **5**, and **7** forms a H-bond with either Gln_{92} (compounds **4** and **5**) or Asn_{62} (compound **6**), and the acyl oxygen of **5** and **7** forms a hydrogen bond with Asn_{62} and Gln_{92}, respectively. The C-4 acyl groups form a network of hydrophobic interactions with Phe_{130}, Leu_{197}, Val_{121}, and/or Pro_{201} and a hydrogen bond with Gln_{92} (except compound **7**). For compound **7**, the distance from the side chain of Phe_{130} to the C-4 acyl group CH_3 is 2.89 Å, which is considerably smaller in value relative to the other compounds where the respective atoms are separated by at least 3.79 Å. The initial difference density clearly showed the position of the Zn^{2+} ion, surrounding water molecules, and each atom of the bound ligand. On the basis of the difference density, we were able to confidently identify the composition of the bound ligand and model its conformation in the active site of hCA II. Figure 3 shows the final $2F_o - F_c$ density for the bound ligand and Zn^{2+} ion. A summary of ligand interactions with hCA II is presented in Table 3. For the data sets reported here, there was no ambiguity as to the presence of hydrolyzed ligands in the active site cleft. The data collection and

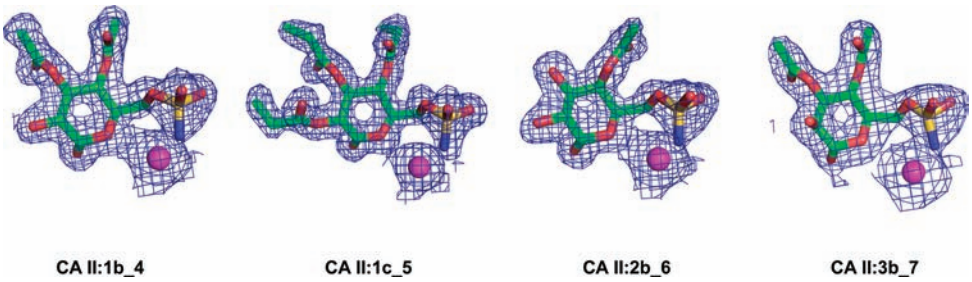

Figure 3. Crystal structures of human CA II in complex with sulfamates **1b** (compound **4**), **1c** (compound **5**), **2b** (compound **6**), and **3b** (compound **7**). Shown are the ligand conformations in the active site. The protein is not shown for clarity. The catalytic zinc ion is colored magenta. The final $2F_o - F_c$ density is contoured in blue at 1σ. The figure was prepared with PyMol.[11].

Table 3. Summary of Ligand Interactions with Protein Residues in hCA II/Ligand Complex Crystal Structures[a]

ligand	4	5	6	7
Direct hydrogen bonds[b]	5	4	6	5
H_2O hydrogen bonds[b]	1	1	1	1
vdW interactions[c]	4	6	4	3

[a] The canonical sulfonamide and sulfamate interactions are not included. [b] Only bond distances below 3.5 Å were considered. [c] Only bond distances below 4.5 Å were considered.

refinement statistics of inhibitor-bound hCA II crystal structures are provided in Supporting Information. The majority of publications that describe structures of hCA II annotate residue numbers that are offset by one relative to the amino acid sequence of hCA II. This may be a consequence of the numbering scheme used in the early hCA II crystal structures (PDB accession codes 1CA2, 2CBB) that skip residue number 126. In this study, we have applied a residue numbering scheme that is in accordance with the amino acid sequence of hCA II.

hCA II is a well studied model enzyme and many assays for measuring enzymatic activity, thermodynamic parameters, or kinetic parameters for binding of inhibitors or substrates to CA are reported.[1b] Assays are typically based on indirect reporters, for example, the emission of light (e.g., fluorescence) or heat change (e.g., ITC). There are no assays designed to discern if a compound is both an inhibitor and a substrate of CA. An assay that allows us to directly observe structural features of CA−inhibitor binding interactions is needed to further assess our crystallography-based findings. Electrospray ionization mass spectrometry (ESI−MS) has been used to study proteins and complexes of proteins with naturally occurring substrates, inhibitors, and drugs.[12] It is generally straightforward to adjust the parameters of the ESI−MS measurement so that the signals observed in the mass spectrometer for a protein and the noncovalent complexes thereof reflect these species in solution.[12] Thus, if an inhibitor is combined with its target enzyme under native state conditions, then the noncovalent complex of [enzyme + inhibitor] may be observed in the ESI mass spectrum. The mass difference ($\Delta m/z$) between the peaks for the unbound [enzyme] and the noncovalent complex [enzyme + inhibitor] can be multiplied by the charge state to give directly the molecular weight of the binding ligand, i.e., $MW_{ligand} = \Delta m/z \times z$ to provide confirmation of the identity of the bound inhibitor.

We and others have previously demonstrated that electrospray ionization−Fourier transform ion cyclotron resonance−mass spectrometry (ESI−FTICR−MS) allows the direct observation of CA in complex with CA inhibitors, and have developed this bioaffinity mass spectrometry methodology (BAMS) to screen for novel CA inhibitors.[13] The FTICR technique allows highly accurate mass measurements. This feature is of great benefit in determining the identity of the unknown binding species in noncovalent protein−ligand complexes.[12] We recently identified a novel class of CA inhibitors belonging to the coumarin chemotype using BAMS.[7a] In that study, a natural product coumarin, 6-(1*S*-hydroxy-3-methylbutyl)-7-methoxy-2*H*-chromen-2-one (**8**), displayed significant CA inhibition. With the use of protein X-ray crystallography, the lactone of **8** was not observed, and instead, its hydrolysis product, the *cis*-2-hydroxy-4-(1*S*-3-methylbutyl)-3-methoxy-cinnamic acid **9**, fitted the electron density, Scheme 3. With BAMS, it was confirmed that the CA bound ligand had an increased molecular weight of 18 Da compared to **8**, consistent with the mass of the hydrolyzed coumarin **9**. A number of follow-up studies confirmed that the zinc bound hydroxide anion of the CA enzyme was responsible for the hydrolysis of the lactone ring of **8**.[7a]

The BAMS method has proven to be a valuable biophysical screening method as it allows the direct observation of the inhibitor with the protein and appears ideal to further assess the unexpected crystallographic observations of the sulfamates. We acquired the positive ion mass spectrum of a solution of hCA II (3.4 μM) in 10 mM NH_4OAc, pH 7.2, using ESI−FTICR−MS,

Scheme 3. The Lactone of the Coumarin Natural Product CA Inhibitor Is Hydrolyzed by hCA II

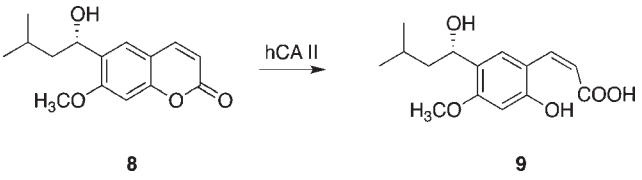

8 **9**

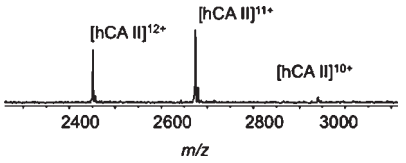

Figure 4. ESI mass spectra of hCA II obtained under native-state conditions. Peaks corresponding to the 12^+ to 10^+ charge states of hCA II are observed.

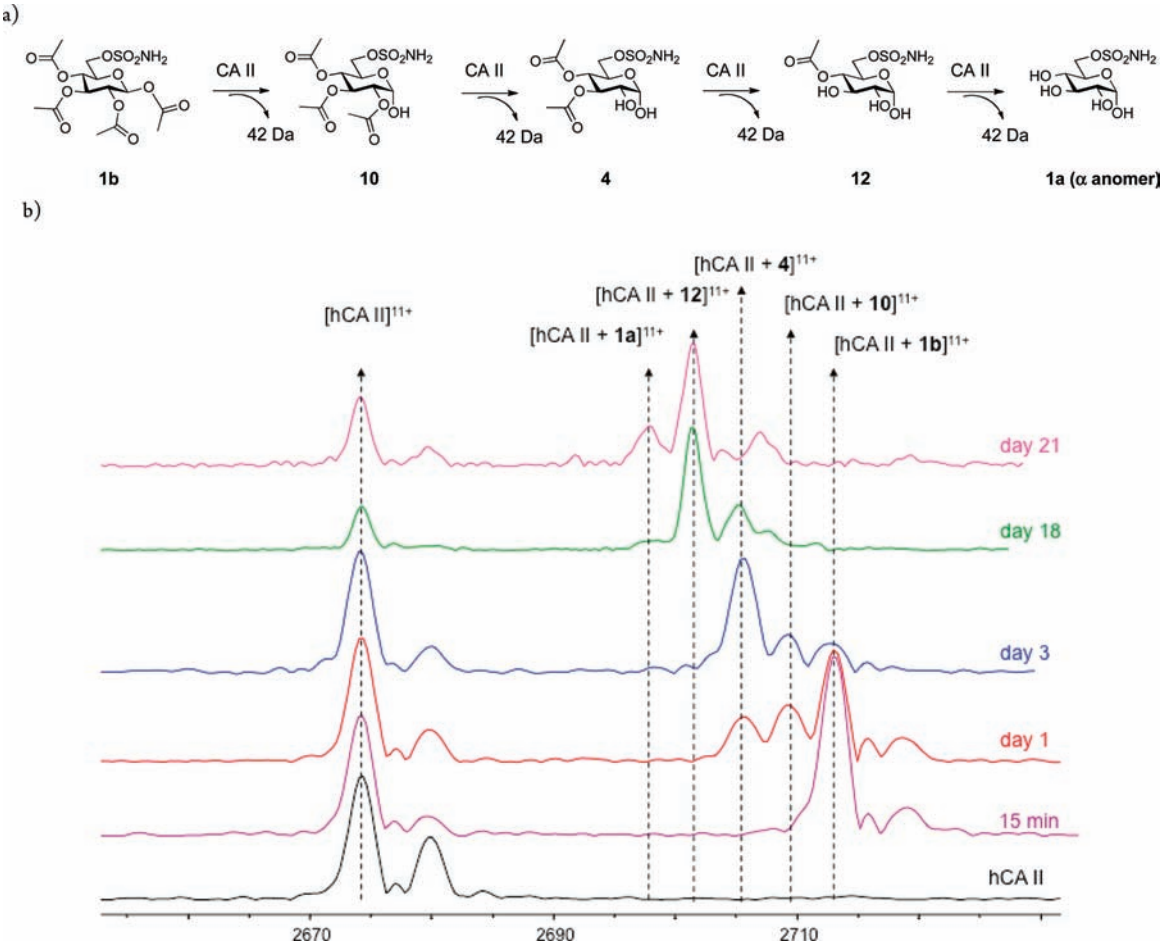

Figure 5. Sequential hydrolysis of acetyl groups from compound **1b** in the presence of hCA II. (a) Possible hydrolysis reaction sequence; (b) ESI mass spectra of hCA II (black trace) and hCA II incubated with **1b** (colored traces) obtained under native-state conditions following incubation for 15 min to 21 days. (Only the 11^+ charge state is shown for clarity.)

Figure 4. Peaks corresponding to the 12^+ to 10^+ charge states of hCA II were observed, and this narrow m/z distribution is indicative of fully folded (native state) hCA II protein.[13d]

Next, we studied a solution of hCA II in the presence of sulfamate inhibitor **1b**. Mass spectra were acquired with this sample following incubation at 16 °C (the same temperature as used for protein co-crystallization) for 15 min, and 1, 3, 18, and 21 days. This analysis yielded the series of mass spectra shown in Figure 5b. These spectra show that with increasing incubation time the sequential loss of 42 Da from the hCA II/ligand noncovalent complex is observed. This mass loss is consistent with the sequential loss of acetyl groups from **1b** to give hydrolyzed ligands **10**, **4**, **12**, and **1a**, Figure 5a. The 15 min incubation yielded the ESI positive ion mass spectrum of Figure 5b, purple trace (only the 11^+ charge state is shown for clarity). In this spectrum, peaks corresponding to unbound hCA II and hCA II—**1b** complex are observed. The ESI positive ion mass spectrum of Figure 5b, red trace, was obtained following a one day incubation time. In this spectrum, peaks corresponding to unbound hCA II and three different noncovalent complexes of hCA II are observed: the latter correspond to [hCA II + **1b**] as well as the loss of one acetate group [hCA II + **10**] and loss of two acetate groups [hCA II + **4**]. Similarly, the ESI mass spectra were acquired after three days (Figure 5b, blue trace), 18 days (Figure 5b, green trace), and 21 days (Figure 5b, pink trace). After three days, the [hCA II + **4**] complex predominated, with much less of [hCA II + **1b**] and [hCA II + **10**] compared to day 1. The [hCA II + **4**] corresponds to the complex observed by protein X-ray crystallography (above; data set hCA II/**1b**_**4**). After 18 days, the [hCA II + **12**] complex predominated, and this corresponds to hydrolysis of three actetate groups from the parent sulfamate **1b**. After 21 days, the [hCA II + **12**] complex continued to predominate, but also evident was the presence of a complex that corresponds to the hydrolysis product of removal of all four acetates of the ligand **1b** (i.e., compound **1a**) to give the complex [hCA II + **1a**]. The mass values of the peaks observed and calculation of the mass of the hCA II bound ligands are provided in the Supporting Information.

We then synthesized compound **10**, the derivative of **1b** where the C-1 anomeric hydroxyl group is deacetylated to give an alcohol as an anomeric α/β mixture in a ratio α/β of 6:4. The BAMS studies demonstrate that compound **1b** is not hydrolyzed following 15 min of incubation; however, after one day, both **1b** and hydrolysis products **10** and **4** are bound to hCA II, while the fully deprotected α anomer of **1a** appears after 21 days. Our CA enzyme inhibition assay includes a preincubation period of 15 min of CA with test inhibitor as this is sufficient time to allow formation of a standard CA—inhibitor complex to allow the inhibition constant (K_i) to be determined. The BAMS studies demonstrate that the hCA II assay result for **1b** (K_i = 307 nM)

dx.doi.org/10.1021/ja207855c |*J. Am. Chem. Soc.* 2011, 133, 18452–18462

determined after 15 min preincubation is indeed due to inhibition by the **1b** parent structure. To afford further insight into the crystallography and BAMS observations, we have elaborated on the enzyme assays of **1b** as well as the deacetylated derivative of **1b**, newly synthesized compound **10**. Assays were performed in which hCA II was preincubated with **1b** or **10** for 15 min, 24, or 72 h at either 4 or 25 °C prior to performing the enzyme inhibition assay, and results are given in Table 4. Comparing Table 4, entry 1 with entries 2−4, shows that the inhibition constant for **1b** decreases with time from K_i = 307 nM (15 min preincubation) to $K_i \sim$ 100 nM (24 h + preincubation at either 4 or 25 °C). These results suggest that the hydrolysis products of **1b** are better inhibitors of hCA II than the parent **1b** structure. Compound **10** (K_i = 50 nM, Table 4, entry 5) and compound **1a** (K_i = 82 nM, Table 4, entry 6) are 6-fold and 3.7-fold more potent than **1b**, respectively, when a 15 min preincubation period is applied. These measured K_i values are consistent with the CA-mediated hydrolysis of **1b** leading to higher potency hCA II inhibitors.

The stopped-flow together with the BAMS measurements demonstrated that the carbohydrate-based sulfamates are both substrate and inhibitor for hCA II. The crystallography data reveal the binding mode for inhibition of several hydrolyzed compounds, but do not show in what conformation the substrate needs to bind to undergo the hydrolysis reaction. To investigate substrate binding in atomic detail, we performed molecular dynamics (MD) simulations of structural models of the substrate **1b** in complex with hCA II, generated with docking tools.[14] Of all docked conformations, only those in which the hydroxide oxygen and a carbonyl carbon of **1b** were in close contact were selected, Figure 6. During the MD simulations, the complexes were stable, with the zinc-bound hydroxide in close proximity to one or more carbonyl carbons of the ester groups.

We further assessed the stability of the modeled substrate−enzyme complex by calculating the noncovalent binding affinity, Table 5. Under the assumption that the docked complexes are representative of reactive conformations, there is a weak tendency for the parent compound **1b** to bind as a substrate for hydrolysis, with a binding constant of 1.34 mM. Note that, for a full analysis of the binding affinity, the covalent interaction, the second step in the reaction mechanism, should also be accounted for. This step is characterized by the nucleophilic attack of the hydroxide on the carbonyl carbon, but is currently computationally inaccessible. To put the calculated dissociation constant into perspective, we repeated the docking and free energy calculation with an activated and a nonactivated ester, *p*-nitrophenyl acetate and phenyl acetate, respectively, for which the esterase activity of hCA II has been measured.[3b] We find that the noncovalent dissociation constant for the hCA II−**1b** complex is orders of magnitude lower than for hCA II in complex with the known

Table 4. Time Dependent Inhibition K_i Data of hCA II with Carbohydrate-Based Sulfamate 1b, and Its Deacetylated Analogues 10 and 1a

entry	compound	preincubation time and temperature	K_i (nM)[a]
1	**1b**	15 min, 25 °C	307
2	**1b**	24 h, 4 °C	113
3	**1b**	72 h, 4 °C	110
4	**1b**	72 h, 25 °C	101
5	**10**	15 min, 25 °C	50
6	**1a**	15 min, 25 °C	82

[a] Errors in the range of ±5% of the reported value, from three determinations; human (cloned) isozymes.

Table 5. Binding free energies and dissociation constants for ligands in a pure inhibitor binding mode and substrate binding mode

substrate binding mode	$\Delta G_{bind}{}^0$ (kJ mol^{-1})	k_d
neutral **1b**	−16.5 ± 0.62	$1.34 \times 10^{-3} \pm 0.13 \times 10^{-3}$
phenyl acetate	10.29 ± 0.23	62.9 ± 3.5
p-nitrophenyl acetate	10.86 ± 0.86	78 ± 15
inhibitor binding mode	$\Delta\Delta G_{bind}$ (kJ mol^{-1})	$k_d{}^4/k_d{}^{1b}$
1b → 4	−39.25 ± 3.08	6.58×10^6

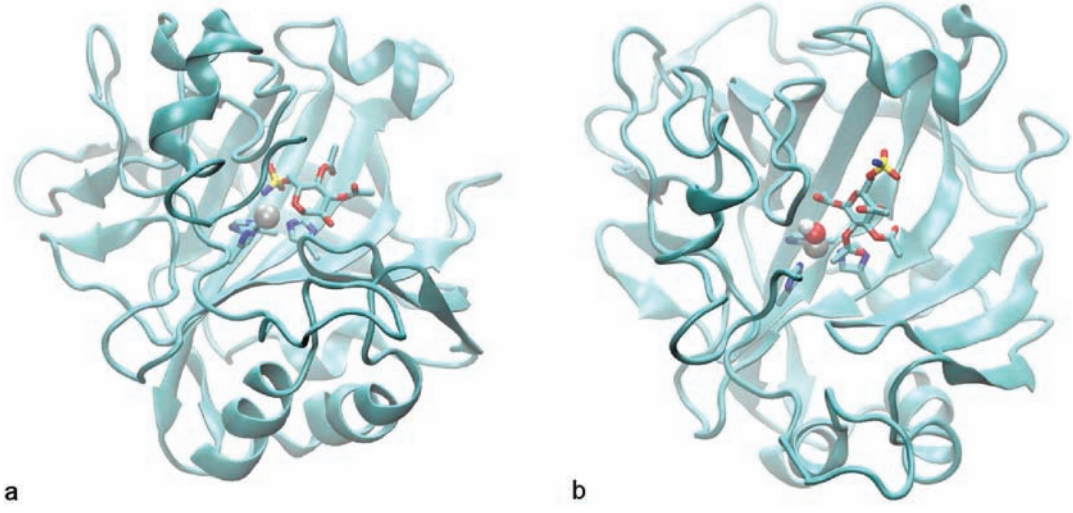

Figure 6. Active site structure of hCA II with the ligand inside the pocket. (a) Pure inhibitor conformation of compound **4** (X-ray structure **CA II:1b_4**) and (b) substrate conformation of the parent sulfamate **1b** (docking structure). Highlighted are the zinc (gray sphere), hydroxide (red-white spheres), ligand (licorice), and histidine residues (licorice in the background).

Scheme 4. Two-State (A) and Three-State (B) Models for the Association of Arylsulfonamides with CA[a]

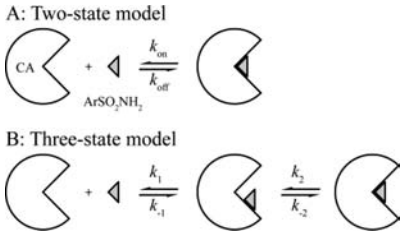

[a] Reprinted from Krishnamurthy, V. M.; Kaufman, G. K.; Urbach, A. R.; Gitlin, I.; Gudiksen, K. L.; Weibel, D. B.; Whitesides, G. M. Carbonic Anhydrase as a Model for Biophysical and Physical-Organic Studies of Proteins and Protein−Ligand Binding. *Chem. Rev.* **2008**, *108*, 946−1051. Copyright 2008 American Chemical Society.

substrates. This strongly suggests that also **1b** can be hydrolyzed by hCA II, even when the catalytic rate for **1b** turns out to be lower than in the case of the known substrates.

To estimate the effect of the hydrolysis on the binding as the inhibitor, we computed the difference in binding free energy ($\Delta\Delta G$) of the inhibitor before (compound **1b**) and after two hydrolysis steps (compound **4**). In these simulations, **1b** was assumed to bind in the same conformation as observed in the X-ray structure of the hCA II−compound **4** complex described above (PDB accession code 3T82). Note that due to the covalent bond between the zinc and the sulfamate we cannot calculate the absolute binding free energy for the inhibitor binding mode and therefore focused on the $\Delta\Delta G$. The results of these calculations show that **4** binds much stronger than **1b** ($\Delta\Delta G = 39$ kJ mol^{-1}). This large difference in binding affinity between **1b** and **4** does not account for the small differences in the measured inhibition constants in Table 5. Therefore, we can speculate that species **1b** does not bind as an inhibitor, but rather as a substrate. This is also supported by the favorable calculated substrate binding affinity and may explain why no X-ray structures were found for the CA II−**1b** complex.

Whitesides and co-workers recently reviewed the kinetics of association and dissociation of CA inhibitors with a sulfonamide ZBG to hCA II.[1b] This analysis showed that $ArSO_2NH_2$ compounds fit both a two-state or a three-state model (Scheme 4). In the two-state model, the $ArSO_2NH_2$ associates with hCA II and coordinates to the active site Zn^{2+} in one step, while in the three-state model, the $ArSO_2NH_2$ first associates with the hCA II to form a noncoordinated complex, that in a second step coordinates to the Zn^{2+}. A number of experimental results were described that supported the three-state model. Our findings with the carbohydrate-based sulfamates are also consistent with the three-state model as these compounds necessarily bind to the CA active site as either a substrate (sulfamate not coordinated to Zn^{2+}) or as an inhibitor (sulfamate is coordinated to Zn^{2+}).

The C-1 acyl group of the four parent sugar sulfamates is equatorial, while the C-1 hydroxyl group was observed axial to the carbohydrate ring for **1b**, **2b**, and **3b** (compounds **4**, **6**, and **7**) and was observed 95% axial and 5% equatorial for **1c** (compound **5**). Hydrolysis of the sugar acyl groups can occur via acyl-oxygen cleavage as in Scheme 1; however, this does not account for the inversion of configuration observed at C-1 in the X-ray crystal structures. A mechanism that is consistent with the almost exclusive formation of the axial hydroxyl from the anomeric acyl group is suggested in Scheme 5 (showing inhibitor/substrate **1b** as an example). Here, hydrolysis occurs via alkyl-oxygen cleavage with formation of the oxocarbenium resonance stabilized cation and departure of the zinc coordinated acyl group. The zinc bound hydroxyl then reacts with the oxocarbenium cation leading to the axial anomer **4** and zinc bound acetate. The acetate is displaced by water and the active CA with zinc bound hydroxyl is regenerated. The formation of a small amount of the equatorial anomer in the case of **1c** could be due to competitive hydrolysis via the two mechanisms (Schemes 1 and 5) or anomerization following alkyl-oxygen cleavage (Scheme 5). The sequential hydrolysis of acyl groups around the ring may be due to a proximity effect: after hydrolysis of the most labile acyl group at C-1, the Zn center is "ready" to bind to the next nearest carbonyl group.

In conclusion, we have demonstrated that per-*O*-acylated sugar-based sulfamates are both substrate and inhibitor for hCA II. This research grew from the initial observations with protein/ligand structures obtained by X-ray crystallography that unexpectedly revealed the hydrolyzed ligands (compounds **4**, **5**, **6**, and **7**) in place of the expected parent ligands **1b**, **1c**, **2b**, and **3b**, respectively. The stopped-flow together with the BAMS measurements then demonstrated that the carbohydrate-based sulfamates are both substrate and inhibitor for hCA II. To investigate what conformation the substrate needs to bind hCA II to undergo the hydrolysis reaction, we next performed MD simulations of structural models of the substrate **1b** in complex with hCA II. Mechanistically, the ester hydrolysis is mediated by the zinc-bound hydroxyl and we can speculate that the fully acylated sugar-based sulfamates do not bind as an inhibitor, but rather as a substrate. The application of esters as a prodrug strategy to mask polar hydroxyl groups is prevalent across medicinal chemistry.[15] The prodrugs often survive the gastrointestinal tract and are absorbed into the bloodstream where they are then hydrolyzed by nonspecific plasma esterases.[16] We employed esterification of the hydroxyl groups of carbohydrate-based sulfamates to modulate their activity as CA inhibitors. While these sulfamates are expected to be substrates of nonspecific esterases, they unexpectedly proved to be substrates of the esterase activity of CAs, their target enzyme class. The implications of CAs as a key contributor to nonspecific esterase activity has not been described previously in a therapeutic context and this study may be a clue to the physiological relevance of the esterase activity of CAs, which is presently unknown.

EXPERIMENTAL SECTION

Protein Crystallography. Human recombinant carbonic anhydrase II (CA II) was expressed in bacteria and crystallized as described previously.[17] Ligand-bound crystals were obtained by co-crystallization with 10 mM ligand (added from a 60 mM stock solution in MeOH). Crystals were immersed in cryoprotectant (25% glycerol in mother liquor with 10 mM ligand). X-ray diffraction results of ligand-bound CA II were obtained at the Australian Synchrotron beamline MX1 (equipped with a Quantum ADSC CCD detector). Data sets were indexed with XDS[18] or Mosflm,[19] and scaling, truncation, and analysis were performed with programs from the CCP4 suite.[20] The structures were determined using difference Fourier techniques and refined with Phenix.[21] Ligand topology was generated with PRODRG,[22] and manual model building and visual inspection were performed with O[23] and

Scheme 5. Proposed Mechanism for the Anomeric Acyl Group Hydrolysis of 1b, 2b, 3b, and 1c by Alkyl Oxygen Cleavage (Showing Inhibitor/Substrate 1b as an Example)

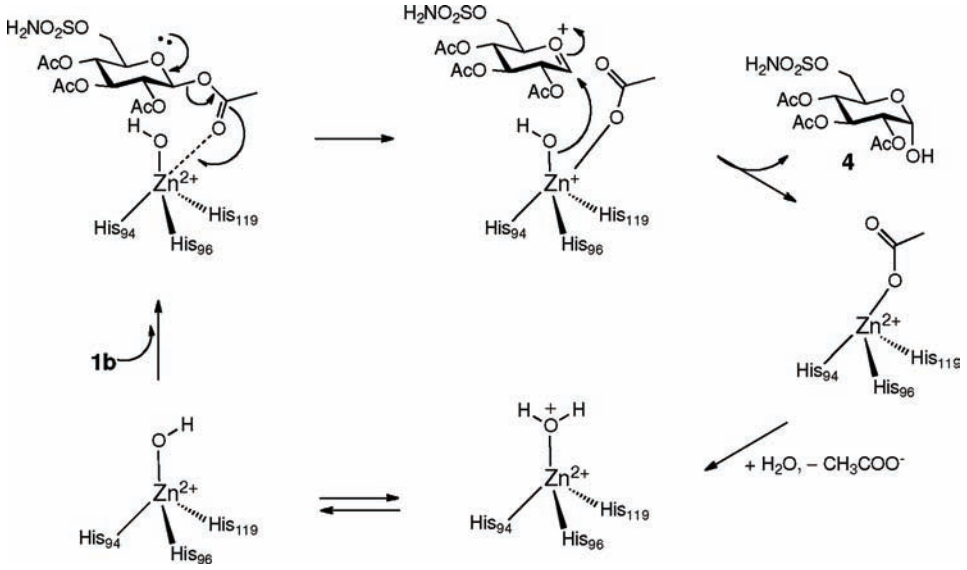

Coot.[24] Coordinates and structure factors have been deposited with the PDB (accession codes 3T82, 3T83, 3T84, and 3T85).

Mass Spectrometry. Mass spectrometry was performed on an APEX III 4.7 T FTICR mass spectrometer (Bruker Daltonics, Billerica, MA) fitted with an Apollo electrospray ionization (ESI) source operated in positive ion mode. XMASS NT V6.1.2 mass spectrometry software on a PC platform was used for data acquisition. Broadband excitation was used to analyze a mass range of m/z 50−6000 and each spectrum was an average of 64 transients (scans) with 512K data points acquired in low resolution mode, with an acquisition time of approximately 4 min/sample. Samples were infused into the ESI source at 2 μL/min. Nitrogen was used as both the drying gas (125 °C) and nebulizing gas. Relevant parameters include a 10^4-fold pressure reduction between source and analyzer regions with an ESI source pressure (10^{-6} mbar) and high vacuum analyzer region pressure (6×10^{-10} mbar). Agilent ESI tuning mix (Santa Clara, CA) was used for an external three-point calibration. The hexapole ion accumulation time was 3 s. Samples for MS analysis were prepared as follows: 3.23 μM hCA II and 11.69 μM (3.6 equiv) ligand **1b** in a total volume of 500 μL. Samples were incubated at 16 °C for 15 min, and 1, 3, 18, and 21 days prior to MS analysis.

Chemical Synthesis, General. All starting reagents were purchased from commercial suppliers. Reactions were monitored by TLC. TLC plates were visualized with UV light and/or orcinol stain (1 g of orcinol monohydrate in a mixture of EtOH/H_2O/H_2SO_4 72.5:22.5:5 mL). Silica gel flash chromatography was performed using silica gel 60 Å (230−400 mesh) from Davisil. ^{1}H NMR were recorded on a Varian Unity 500 MHz spectrometer at 30 °C. Chemical shifts for ^{1}H and ^{13}C NMR run in DMSO-d_6 are reported in ppm relative to residual solvent proton (δ = 2.50 ppm) and carbon (δ = 39.5 ppm) signals, respectively. Multiplicity is indicated as follows: s (singlet); d (doublet); t (triplet); m (multiplet); dd (doublet of doublet); ddd (doublet of doublet of doublet); br (broad). Coupling constants are reported in hertz (Hz). Melting points measured on a Cole Parmer instrument are uncorrected. High-resolution electrospray ionization mass spectra were performed on an Apex III Bruker Daltonics 4.7T Fourier transform mass spectrometer (FTMS) fitted with an Apollo ESI source. Low resolution mass spectra were acquired on an Applied Biosystems Pty Ltd. Mariner ESI-TOF mass spectrometer using electrospray as the ionization technique in positive ion and/or negative ion modes as stated. All MS analysis samples were prepared as solutions in methanol. Compounds **1a**−**3a**, **1b**−**3b**, **1c**, and **1d** were synthesized as reported previously by our group.[9]

Synthesis of 2,3,4-Tri-*O*-acetyl-6-sulfamoyl-α,β-D-gluco-pyranose (10)[25]. Hydrazine acetate (24 mg, 0.27 mmol, 1.3 equiv) was added to a solution of compound **1b** (91 mg, 0.21 mmol, 1.0 equiv) in DMF (1 mL) at 75 °C. The reaction was stirred for 20 min at 75 °C, then diluted in EtOAc (20 mL), washed with brine (×2), and the aqueous fractions back extracted with EtOAc (×2). The organic fractions were then combined, dried over $MgSO_4$, filtrated, and the solvent evaporated leaving a crude residue that was purified by flash chromatogaphy (1:1 EtOAc/hexane) to afford the title compound **10** (66 mg, 0.17 mmol, 81% yield, α/β 6/4) as a white solid. mp = 147 °C. R_f = 0.28 (3:2 EtOAc/hexane). ^{1}H NMR (500 MHz, DMSO-d_6): δ = 7.53 (br s, 2H, NH_2); 7.36 (d, J = 6.0 Hz, 0.4H, OH-1$_\beta$); 7.33 (d, J = 4.5 Hz, 0.6H, OH-1$_\alpha$); 5.36 (t, J = 10.0 Hz, 0.6H, H-3$_\alpha$); 5.25 (t, J = 10.0 Hz, 0.4H, H-3$_\beta$); 5.25 (t, J = 4.0 Hz, 0.6H, H-1$_\alpha$); 4.90 (t, J = 10.0 Hz, 0.6H, H-4$_\alpha$); 4.89 (t, J = 7.0 Hz, 0.4H, H-1$_\beta$); 4.83 (t, J = 9.5 Hz, 0.4H, H-4$_\beta$); 4.73 (dd, J = 10.0, 3.5 Hz, 0.6H, H-2$_\alpha$); 4.71 (dd, J = 10.0, 8.0 Hz, 0.4H, H-2$_\beta$); 4.19 (m, 0.6H, H-5$_\alpha$); 4.05−4.01 (m, 2.4H, H-5$_\beta$, H-6a, H-6b); 2.02, 2.01, 1.99, 1.97, 1.94 (5 × s, 9H, OCOCH_3), assignments were confirmed by ^{1}H−^{1}H gCOSY. ^{13}C NMR (125 MHz, DMSO-d_6): δ = 170.2, 170.1, 169.7 (OCOCH$_3$); 94.1 (C-1$_\beta$); 89.3 (C-1$_\alpha$); 72.7 (C-2$_\beta$); 72.6 (C-3$_\beta$); 71.0 (C-2$_\alpha$); 70.6 (C-5$_\beta$); 69.7, 69.7 (C-3$_\alpha$, C-4$_\alpha$); 68.8 (C-4$_\beta$); 68.7 (C-5$_\alpha$); 67.5 (C-6$_\beta$); 66.6 (C-6$_\alpha$); 20.7, 20.6, 20.5 (OCOCH$_3$), assignments were confirmed by ^{1}H−^{13}C HSQC. LRMS (ESI$^+$): m/z = 408 [M + Na]$^+$. HRMS: calcd for $C_{12}H_{19}NO_{11}SNa$ 408.0571, found 408.0577.

Carbonic Anhydrase Catalytic Inhibition Assays. An SX.18MV-R Applied Photophysics stopped-flow instrument has been used for assaying the CA II CO_2 hydration activity. Phenol red (at a concentration of 0.2 mM) has been used as indicator, working at the absorbance maximum of 557 nm, with 10 mM Hepes (pH 7.5) as buffer, 0.1 M $NaClO_4$ (for maintaining constant the ionic strength, this anion is not inhibitory), following the CA-catalyzed CO_2 hydration reaction for a period of 10−100 s. Saturated CO_2 solutions in water at 20 °C were used as substrate. Stock solutions of inhibitors were prepared at a concentration of 10−50 mM (in the assay buffer) and dilutions up to 1 nM done with the assay buffer mentioned above. Inhibitor and enzyme solutions

were preincubated together for the required time at room temperature prior to assay, in order to allow for the formation of the E-I complex and time for the acyl group hydrolysis. The inhibition constants were obtained by nonlinear least-squares methods using PRISM 3. The curve-fitting algorithm allowed us to obtain the IC_{50} values, working at the lowest concentration of substrate of 1.7 mM), from which K_i values were calculated by using the Cheng−Prusoff equation. The catalytic activity (in the absence of inhibitors) of these enzymes was calculated from Lineweaver−Burk plots and represent the mean from at least three different determinations. The hCA II enzyme concentration was 10.3 nM.

Free-Energy Calculations. *Simulation Setup.* All simulations were performed using the Gromacs software package.[26] The md integrator was used. All bonds were constrained using the LINCS algorithm,[27] allowing a time step of 2 fs. The temperature was connected to a heat bath of 300 K via the v-rescale thermostat.[28] The pressure was maintained constant at 1 atm using the Parrinello−Rahman barostat with τ_p set to 1.0 and the compressibility to 4.5×10^{-5}.[29] van der Waals interactions were switched off between 0.8 and 0.9 and a dispersion correction term was included. The electrostatic interactions were treated using PME[30] with a real space cutoff of 1.0 nm. The simulation box was generated by creating a dodecahedron box around the protein and/or ligand, with a minimum distance of 1.0 nm between the box and the solute. The rest of the box was filled with TIP3P[31] water molecules and Na^+ and Cl^- atoms were added to obtain a neutral box of approximately 0.1 M. The resulting system was energy minimized by steepest descent and simulated for 1 ns with position restraints on the protein and/or ligand.

We have used the Amber force fields for our simulations, with the Amber99sb parameter set for the protein. The parameters for the active site were taken from Suárez et al.[32] To describe the carbohydrate ligands, we used the carbohydrate optimized Glycam06 parameter set.[33] The missing parameters for the sulfamate were taken from the Gaff parameter set.[34] To describe the phenyl acetate, *p*-nitrophenyl acetate, we used the Gaff parameter set. For all ligands, the derivation of the charge set was done following the Glycam06 procedure. Glycam06 was preferred over Gaff, because all atom charge fitting leads to overfitting of the electrostatic potential.[35] Removing the aliphatic hydrogens from the fit will reduce the chance of overfitting without large effects for the charge distribution of the molecule.[33] The charges we used for the ligands and the active site are provided as Supporting Information.

Inhibitor Binding Free-Energy Difference. The binding free energy of the ligand in the inhibitor binding mode cannot be calculated directly, because the sulfamate nitrogen is chemically bonded to the zinc of the hCA II active site. The energy of a chemical bond cannot be assessed in a classical MD simulation, and consequently, the associated binding free energy cannot be calculated. Therefore, we calculated the free-energy difference between ligand **1b** and compound **4** in water and in the protein. These are related to the binding free energies through the thermodynamic cycle displayed in Figure 7.

Then, $\Delta\Delta G_{bind} = \Delta G^{4}_{bind} - \Delta G^{1b}_{bind} = \Delta G_{hyd.prot} - \Delta G_{hyd.wat}$. The difference in binding free energy $\Delta\Delta G_{bind}$ is then related to the ratio of the dissociation constants through $k^4_d/k^{1b}_d = \exp(-\Delta\Delta G_{bind}/RT)$. The free-energy differences $\Delta G_{hyd.prot}$ and $\Delta G_{hyd.wat}$ were computed using the Crooks Gaussian intersection method (CGI)[36] and the error is estimated as described.[33] For the short simulations, to calculate the work to change **1b** into **4** and vice versa, the van der Waals switching parameters were changed to 1.0 and 1.1 nm and the PME real space cutoff to 1.2 nm. For $\Delta G_{hyd.wat}$, morphing one state into the other was done within 50 ps. This was repeated 100 times with different starting conformations obtained from at least 10 ns equilibrium trajectory. For $\Delta G_{hyd.prot}$, the same procedure was followed with morphing times increased to 1 ns to obtain reasonable accuracy.

Ester Hydrolysis by hCA II. We used Flexx[14] to dock neutral **1b**, phenyl acetate, and *p*-nitrophenyl acetate into the active site of hCA II. The initial protein structure for the docking was the X-ray structure PDB ID

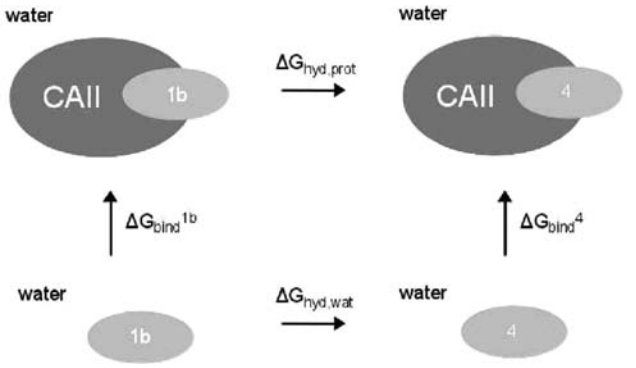

Figure 7. Free energy cycle used to calculate the difference in binding free energy between compound **4** and **1b** ($\Delta\Delta G_{bind} = \Delta G^{4}_{bind} - \Delta G^{1b}_{bind} = \Delta G_{hyd.prot} - \Delta G_{hyd.wat}$).

3T82 (**CA II:1b_4**). After adding hydrogens to this structure, we substituted the ligand N−H (ligated to Zn^{2+}) with O−H and removed all other atoms of the ligand. We defined the binding site as a sphere with a radius of 8 Å around the oxygen of the hydroxide ion. For every ligand, we created the maximum number of docking poses (2000). From the created database of docking poses, we visually inspected the structures. The four highest ranked structures with a unique close contact interaction between the hydroxide ion and the carbonyl carbon of the ester were selected for further investigation. Then, we equilibrated these complexes for 2 ns including position restraints on the ligand Zn^{2+}, OH^- and the three histidine residues coordinated to the Zn^{2+} to allow for side chain equilibration. Finally, a short production run was done without position restraints for 10 ns.

When the ligand is considered as a substrate for ester hydrolysis, there are no bonded interactions between the ligand and the active site. Consequently, we can calculate the binding free energy directly. Therefore, we use discrete thermodynamic integration (DTI) and Bennet Acceptance Ration (BAR)[37] to extract the ligand binding free energy. First, the ligands coulomb interactions are removed in five steps $\lambda = \{0; 0.25; 0.5; 0.75; 1\}$. Then, the van der Waals interactions between the ligand and protein/solvent are removed in 16 steps with $\lambda = \{0; 0.05; 0.1; 0.2; 0.3; 0.4; 0.5; 0.6; 0.65; 0.7; 0.75; 0.8; 0.85; 0.9; 0.95; 1\}$. The spacing between the λ-points is chosen to have sufficient overlap between two neighboring points. This procedure was performed for the ligand in water and in the protein to obtain the binding free energy. To maintain the average bonded conformation of the ligand in the protein, we introduced position and orientation restraints acting on the ligand with respect to the protein.[38] These restraints were introduced in three steps $\lambda=\{0; 0.5; 1\}$. Furthermore, a standard state correction was applied.[38] For these simulations, the md integrator was replaced by the sd integrator[39] with the reference temperature set to 300 K. This ensured appropriate sampling of the decoupled state. The van der Waals switching parameters were changed to 1.0 and 1.1 nm and the PME real space cutoff to 1.2 nm.

Abbreviations. ESI−FTICR−MS, electrospray ionization−Fourier transform ion cyclotron resonance−mass spectrometry; CA, carbonic anhydrase; ZBG, zinc binding group; PDB, Protein Data Bank; SAR, structure−activity relationships; BAMS, bioaffinity mass spectrometry; MD, molecular dynamics.

■ ASSOCIATED CONTENT

Supporting Information. Data collection and refinement statistics of inhibitor-bound hCA II crystal structures; ESI−FTICR−MS calculated mass values of the peaks observed in the mass spectra; and the charges used for the ligands and the

active site in MD. This material is available free of charge via the Internet at http://pubs.acs.org.

AUTHOR INFORMATION

Corresponding Author
s.poulsen@griffith.edu.au

ACKNOWLEDGMENT

We thank Professor Emeritus Ian D. Jenkins for helpful discussions. cDNA for hCA II was kindly provided by Prof. Carol Fierke. This work was financed by the Australian Research Council (Grant number DP1110071 to S.-A.P.); an EU grant of the 7th framework programme (METOXIA project to C.T.S.). M.G.W. thanks the Humboldt Foundation for financial support. C.K.W. is supported by a NHMRC postdoctoral training Fellowship. We gratefully acknowledge the award of beam time by the Australian Synchrotron.

REFERENCES

(1) (a) Supuran, C. T. *Nat. Rev. Drug Discovery* **2008**, *7* (2), 168–181. (b) Krishnamurthy, V. M.; Kaufman, G. K.; Urbach, A. R.; Gitlin, I.; Gudiksen, K. L.; Weibel, D. B.; Whitesides, G. M. *Chem. Rev.* **2008**, *108* (3), 946–1051.

(2) Babtie, A.; Tokuriki, N.; Hollfelder, F. *Curr. Opin. Chem. Biol.* **2010**, *14*, 200–207.

(3) (a) Krebs, J. F.; Ippolito, J. A.; Christianson, D. W.; Fierke, C. A. *J. Biol. Chem.* **1993**, *268*, 27458–27466. (b) Aharoni, A.; Gaidukov, L.; Khersonsky, O.; McQ Gould, S.; Roodveldt, C.; Tawfik, D. S. *Nat. Genet.* **2005**, *37*, 73–76.

(4) Innocenti, A.; Scozzafava, A.; Parkkila, S.; Puccetti, L.; De Simone, G.; Supuran, C. T. *Bioorg. Med. Chem. Lett.* **2008**, *18*, 2267–2271.

(5) Supuran, C. T. In *Carbonic Anhydrase Its Inhibitors and Activators*; Supuran, C. T., Scozzafava, A., Conway, J., Eds.; CRC Press LLC: Boca Raton, FL, 2004; pp 1−23.

(6) (a) Briganti, F.; Mangani, S.; Scozzafava, A.; Vernaglione, G.; Supuran, C. T. *J. Biol. Inorg. Chem.* **1999**, *4* (5), 528–536. (b) Pocker, Y.; Stone, J. T. *Biochemistry* **1968**, *7*, 3021–31.

(7) (a) Maresca, A.; Temperini, C.; Vu, H.; Pham, N. B.; Poulsen, S.-A.; Scozzafava, A.; Quinn, R. J.; Supuran, C. T. *J. Am. Chem. Soc.* **2009**, *131* (8), 3057–3062. (b) Maresca, A.; Temperini, C.; Pochet, L.; Masereel, B.; Scozzafava, A.; Supuran, C. T. *J. Med. Chem.* **2009**, *53* (1), 335–344.

(8) Gould, S. M.; Tawfik, D. S. *Biochemistry* **2005**, *44*, 5444–5452.

(9) Lopez, M.; Trajkovic, J.; Bornaghi, L. F.; Innocenti, A.; Vullo, D.; Supuran, C. T.; Poulsen, S.-A. *J. Med. Chem.* **2011**, *54* (5), 1481–1489.

(10) Khalifah, R. G. *J. Biol. Chem.* **1971**, *246* (8), 2561–2573.

(11) The PyMOL Molecular Graphics System, Version 1.3, Schrödinger, LLC. http://www.pymol.org.

(12) Hofstadler, S. A.; Sannes-Lowery, K. A. *Nat. Rev. Drug Discovery* **2006**, *5*, 585–595.

(13) (a) Poulsen, S.-A. *J. Am. Soc. Mass Spectrom.* **2006**, *17* (8), 1074–1080. (b) Poulsen, S.-A.; Davis, R. A.; Keys, T. G. *Bioorg. Med. Chem.* **2006**, *14* (2), 510–515. (c) Vu, H.; Pham, N. B.; Quinn, R. J. *J. Biomol. Screening* **2008**, *13* (4), 265–275. (d) Cheng, X.; Chen, R.; Bruce, J. E.; Schwartz, B. L.; Anderson, G. A.; Hofstadler, S. A.; Gale, D. C.; Smith, R. D.; Gao, J.; Sigal, G. B.; Mammen, M.; Whitesides, G. M. *J. Am. Chem. Soc.* **1995**, *117*, 8859–8860.

(14) Rarey, M.; Kramer, B.; Lengauer, T.; Klebe, G. *J. Mol. Biol.* **1996**, *261*, 470–489.

(15) Lavis, L. D. *ACS Chem. Biol.* **2008**, *3*, 203–206.

(16) Di, L.; Kerns, E. H.; Hong, Y.; Chen, H. *Int. J. Pharm.* **2005**, *297*, 110–119.

(17) Lopez, M.; Paul, B.; Hofmann, A.; Morizzi, J.; Wu, Q. K.; Charman, S. A.; Innocenti, A.; Vullo, D.; Supuran, C. T.; Poulsen, S.-A. *J. Med. Chem.* **2009**, *52* (20), 6421–6432.

(18) Kabsch, W. *J Appl. Chrystallogr.* **1993**, *26*, 795–800.

(19) Leslie, A. *Newsletter on Protein Crystallography* **1992**, No. 26.

(20) Collaborative Computational Project Number 4. *Acta Crystallogr., Sect. D: Biol. Crystallogr.* **1994**, *54*, 905-921.

(21) Adams, P. D.; Afonine, P. V.; Bunkócz, i. G.; Chen, V. B.; Davis, I. W.; Echols, N.; Headd, J. J.; Hung, L.; Kapral, G. J.; Grosse-Kunstleve, R. W. *Acta Crystallogr., Sect. D: Biol. Crystallogr.* **2010**, *66*, 213–221.

(22) Schuettelkopf, A. W.; van Aalten, D. M. F. *Acta Crystallogr., Sect. D: Biol. Crystallogr.* **2004**, *60*, 1355–1363.

(23) Jones, T. A.; Zou, J. Y.; Cowan, S.; Kjeldgaard, M. *Acta Crystallogr. Sect. A: Found. Crystallogr.* **1991**, *47*, 110–119.

(24) Emsley, P.; Cowton, K. *Acta Crystallogr., Sect. D: Biol. Crystallogr.* **2004**, *60*, 2126–2132.

(25) Excoffier, G.; Gagnaire, D.; Utille, J.-P. *Carbohydr. Res.* **1975**, *39*, 368–373.

(26) Hess, B.; Kutzner, C.; van der Spoel, D.; Lindahl, E. *J. Chem. Theor. Comp.* **2008**, *4*, 435–447.

(27) Hess, B.; Bekker, H.; Berendsen, H. J. C.; Fraaije, J. G. E. M. *J. Comput. Chem.* **1997**, *18*, 1463–1472.

(28) Bussi, G.; Donadio, D.; Parrinello, M. *J. Chem. Phys.* **2007**, *126*, 014101.

(29) Parrinello, M.; Rahman, A. *J. Appl. Phys.* **1981**, *52*, 7182–7190.

(30) Darden, T.; York, D.; Pedersen, L. *J. Chem. Phys.* **1993**, *98*, 10089–10092.

(31) Jorgensen, W.; Chandrasekhar, J.; Madura, J.; Impey, R.; Klein, M. *J. Chem. Phys.* **1983**, *79*, 926–935.

(32) Suarez, D.; Merz, K., Jr. *J. Am. Chem. Soc.* **2001**, *123*, 3759–3770.

(33) Kirshner, K.; Yongye, A.; Tschampel, S.; Gonzalez-Outeirino, J.; Daniels, C.; Foley, B.; Woods, R. *J. Comput. Chem.* **2008**, *29*, 622–655.

(34) Wang, J.; Wolf, R.; Caldwell, J.; Kollman, P.; Case, D. *J. Comput. Chem.* **2004**, *25*, 1157–1174.

(35) Francl, M.; Carey, C.; Chirlian, L. *J. Comput. Chem.* **1996**, *17*, 367–383.

(36) Goette, M.; Grubmüller, H. *J. Comput. Chem.* **2009**, *30*, 447–456.

(37) Bennett, C. *J. Comput. Phys.* **1976**, *22*, 245–268.

(38) Boresch, S.; Tettinger, F.; Leitgeb, M.; Karplus, M. *J. Phys. Chem. B* **2003**, *107*, 9535–9551.

(39) Van Gunsteren, W.; Berendsen, H. *Mol. Simul.* **1988**, *1*, 173–185.